AIP | Chaos
An Interdisciplinary Journal of Nonlinear Science

In-flight and collisional dissipation as a mechanism to suppress Fermi acceleration in a breathing Lorentz gas

Diego F. M. Oliveira and Edson D. Leonel

Citation: Chaos **22**, 026123 (2012); doi: 10.1063/1.3697392
View online: http://dx.doi.org/10.1063/1.3697392
View Table of Contents: http://chaos.aip.org/resource/1/CHAOEH/v22/i2
Published by the AIP Publishing LLC.

In-flight and collisional dissipation as a mechanism to suppress Fermi acceleration in a breathing Lorentz gas

Diego F. M. Oliveira[1,a)] and Edson D. Leonel[2,b)]
[1]*Max-Planck-Institut für Physik komplexer Systeme, Nöthnitzer St. 38, D-01187 Dresden, Germany; Institute for Multiscale Simulations, Friedrich-Alexander Universität, Naegelsbachstrasse 49b, D-91052 Erlangen, Germany; and CAMTP - Center For Applied Mathematics and Theoretical Physics, University of Maribor, Krekova 2, SI-2000 Maribor, Slovenia*
[2]*Departamento de Estatística, Matemática Aplicada e Computação, UNESP—Univ Estadual Paulista, Ave. 24A, 1515—Bela Vista, 13506-900 Rio Claro, SP, Brazil*

(Received 6 December 2011; accepted 6 March 2012; published online 25 June 2012)

Some dynamical properties for a time dependent Lorentz gas considering both the dissipative and non dissipative dynamics are studied. The model is described by using a four-dimensional nonlinear mapping. For the conservative dynamics, scaling laws are obtained for the behavior of the average velocity for an ensemble of non interacting particles and the unlimited energy growth is confirmed. For the dissipative case, four different kinds of damping forces are considered namely: (i) restitution coefficient which makes the particle experiences a loss of energy upon collisions; and in-flight dissipation given by (ii) $F = -\eta V^2$; (iii) $F = -\eta V^\mu$ with $\mu \neq 1$ and $\mu \neq 2$ and; (iv) $F = -\eta V$, where η is the dissipation parameter. Extensive numerical simulations were made and our results confirm that the unlimited energy growth, observed for the conservative dynamics, is suppressed for the dissipative case. The behaviour of the average velocity is described using scaling arguments and classes of universalities are defined. © *2012 American Institute of Physics*. [http://dx.doi.org/10.1063/1.3697392]

We revisit the problem of non-interacting particles in a time dependent Lorentz gas. We describe the model by using a four dimensional nonlinear map. As it is known, the phase space of the Lorentz gas with static scatterers is fully chaotic and the velocity of the particle is constant. However, when a time dependent perturbation is introduced to the boundary, the energy is no longer conserved and the unlimited energy growth is observed for the conservative case. On the other hand, our results show that when dissipation is introduced into the system, either by collisional dissipation or dissipation during the flight, the unlimited energy growth is no longer observed. Depending on the strength of the dissipation and considering short time, the average velocity can either grows and reaches a constant plateau or decays until the particle reaches the state of rest. For the cases, when the dynamics does not stop between the scatterers, the behaviour of the average velocity is described by using scaling arguments and once the scaling exponents are known, classes of universalities are defined.

I. INTRODUCTION

In 1949, Enrico Fermi,[1] as an attempt to explain the origin of cosmic acceleration, proposed that charged particles could be accelerated by collision/iteraction with time dependent magnetic structures. Since then, many models have been proposed in order to understand Fermi's idea.[2–5] One of the most studied versions of the problem is the one-dimensional Fermi-Ulam model (FUM).[6–10] The model consists basically of a classical particle confined and bouncing between two rigid walls, one of them is assumed to be fixed and the other one moves according to a periodic function. For such a system, it is known that the phase space, in the absence of dissipation, is mixed, in the sense that depending on the combinations of control parameters and initial conditions, Kolmogorov-Arnold-Moser (KAM) islands, invariant spanning curves and chaotic seas are all observed. In such a model, the existence of a set of invariant spanning curves limiting the size of the chaotic sea prevents the unlimited energy growth of the particle.[11–14] On the other hand, an alternative model was proposed by Pustylnikov[15,16] which consists of a classical particle bouncing in a vertical moving platform, having, instead of a fixed wall, an constant gravitational field working as returning mechanism.[17–22] For such a system and for specific combinations of both control parameters and initial conditions, the phenomenon of unlimited energy growth can be observed due to the loss of correlation between two collisions.

A natural extension of the one-dimensional billiard models are the two-dimensional billiard systems.[23–27] From the mathematical point of view, a billiard is defined by a connected region $Q \subset R^D$, with boundary $\partial Q \subset R^{D-1}$ which separates Q from its complement. Basically, they are settled in three classes, namely (i) integrable, (ii) ergodic, and (iii) mixed. In case (i), the phase space consists of invariant tori filling the entire phase space and two examples are the circular[28] and the elliptical.[29] In case (ii), two examples are the Bunimovich stadium[30] and the Sinai billiard,[31] in such a cases, the time evolution of a single initial condition is

a)Electronic mail: diegofregolente@gmail.com.
b)Electronic mail: edleonel@rc.unesp.br.

enough to fill the entire phase space. Finally, case (iii), mixed type systems, in such a case, chaotic seas are generally surrounding KAM islands and invariant curves are observed[32–40] (and references in therein). If a time dependent perturbation is introduced in the boundary, $\partial Q = \partial Q(t)$, the system exchanges energy/velocity with the particle upon collision. Such a type of systems have been studied a lot in the last years in order to understand the phenomenon known as Fermi acceleration i.e., unlimited energy growth.[41] According to the conjecture proposed by Loskutov-Ryabov-Akinshin conjecture[42] (known as LRA conjecture), the existence of a chaotic component in the phase space is a sufficient condition to observe Fermi acceleration when a time dependent perturbation is introduced to the boundary. However, recent results show that the existence of a chaotic component is a sufficient, but not necessary condition for Fermi acceleration since the unlimited energy growth was recently observed for a time dependent elliptical billiard.[43–45] As it is known, the elliptical billiard with static boundary is an integrable system whose the integrability comes from the conservation of energy and the angular momentum with respect to the two foci.[25] However, when time dependent perturbation is introduced into the system, the separatrix is destroyed given place to a stochastic layer and trajectories confined inside the separatrix (librators) can now explore the region outside the separatrix (rotators). This change of behaviour is the mechanism which produces Fermi acceleration.[43] Once the unlimited energy growth is observed, a natural question is *what is the consequence of the introduction of dissipation into the system?* According to the conjecture proposed by Leonel,[46] the phenomenon of Fermi acceleration is not structurally stable and the introduction of dissipation is a sufficient condition to suppress the unlimited energy growth.

In this sense, we revisit the problem of a Lorentz gas seeking to understand and describe some dynamical properties of the average velocity for an ensemble of non interacting particles as a function of both the control parameters and number of collisions of the particles with the boundary. First, we assume two square lattices of disks,[47–49] the distance between the center of the scatterers is fixed and equals to the unity. The scatterers of one of the square lattice have radius r_a, on the other hand, the disks of the second lattice have radius r_b, such as $r_b < r_a$, and they are placed between four scatterers of radius r_a. Additionally, we assume that the center of mass of the scatterers does not move, however, the size of the scatterers increase and decrease according to a periodic function. We call such mode as the breathing geometry. The study is carried out considering the conservative as well as the dissipative dynamics. For the latter, four cases are taken into account, namely, one collisional dissipation and three dissipative laws for the case of in-flight dissipation, namely, (i) $F = -\eta V^2$; (ii) $F = -\eta V^\mu$ with $\mu \neq 1$ and $\mu \neq 2$; (iii) $F = -\eta V$, where η is the dissipation parameter. For all of them, we study the behaviour of the average velocity for an ensemble of non interacting particles. Our results show that for the conservative dynamics, the unlimited energy growth is observed, therefore, confirming the LRA-conjecture. However, for the dissipative dynamics and for some cases and for short number of collisions, the average velocity grows according to a power law and after a characteristic crossover number it remains constant. Therefore, the introduction of dissipation is a sufficient condition to suppress the unlimited energy growth. On the other hand, if the dissipation is strong enough, even for high initial velocities, the average velocity may decays until the particle reaches the state of rest and stop between the scatterers.

The paper is organized as follows. In Sec. II, we describe all the necessary details to obtain the four-dimensional map that describes the dynamics of the system for the conservative as well as the case of collisional dissipation. Section III is devoted to the cases of in-flight dissipation. The four dimensional mapping is obtained and numerical results are discussed. Finally, conclusions are drawn in Sec. IV.

II. A TIME DEPENDENT LORENTZ GAS WITH BREATHING GEOMETRY

In this section, we discuss all the details needed for the construction of a non-linear map that describes the dynamics of the problem. The model consists of a classical particle of mass m experiencing collisions with time dependent circular scatters of two different sizes as shown in Fig. 1. The system is described in terms of a four dimensional mapping $T(\theta_n, b_n, |\vec{V}_n|, t_n) = (\theta_{n+1}, b_{n+1}, |\vec{V}_{n+1}|, t_{n+1})$, where the dynamical variable θ_n denotes the direction of the trajectory; b_n is the impact parameter; $|\vec{V}_n|$ is the absolute velocity of the particle after collision, and t_n is the time. The dynamics starts in the scatter in the center and we specify the scattered hit in the collision $n+1$ by $s_n = 0, ..., 7$ and introduce $l(s_n)$ for the distance of this scatterer and the scatterer hit at the collision $n+1$. $l(s_n)$ can take the values of 1 and $\sqrt{2}$ for even and odd values of s_n for collisions with the scatter with radius $R(t)$ and $\sqrt{2}/2$ for collisions with the scatters with radius $r(t)$. It is important to notice that if after leaving the scatter in the

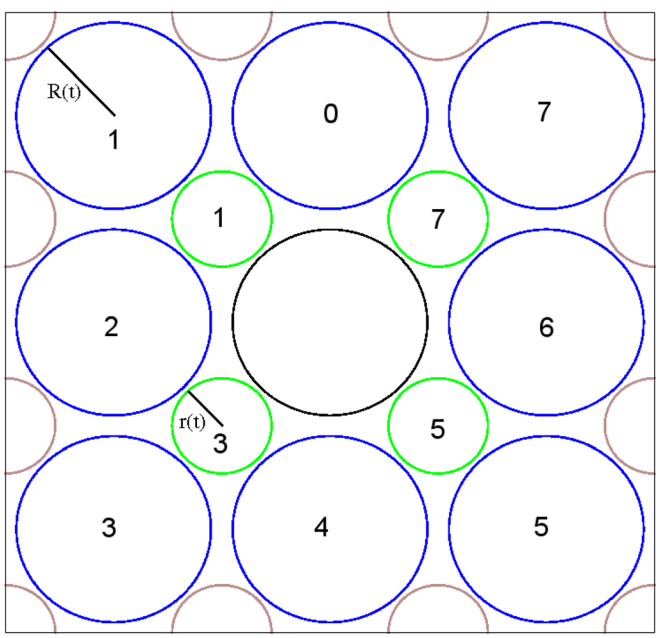

FIG. 1. Illustration of the configuration for the time dependent Lorentz gas.

center (the black one), the particle hits the green scatter [r(t)] for the next collision the reference frame is moved.

There are many different ways to introduce time-dependent perturbation, in particular, we consider the case where the size of each circle increases and decreases periodically in time, we call this as *breathing geometry*. The radii in polar coordinates, are given by

$$R(t) = r_a + \epsilon_1[1 + \cos(t)], \tag{1}$$

$$r(t) = r_b + \epsilon_2[1 + \cos(t)], \tag{2}$$

where ϵ_1 and ϵ_2 are the amplitudes of the time-dependent perturbation, r_a and r_b are constraints such as $r_a > r_b$, and t is the time. We now describe all the details to obtain the mapping. Here, we assume a collision between scatters with $R(t)$ (see Fig. 1), however an extension for collisions between black, $R(t)$, and green scatters, $r(t)$, is straightforward. Assuming that an initial condition $(\theta_n, b_n, |\vec{V}_n|, t_n)$ is given, we can obtain the equation that describes the dynamics of the system. The cartesian components of $R(t_n)$ are given by

$$X(\delta_n, t_n) = \{1 + \epsilon_1[1 + \cos(t_n)]\}\cos(\delta_n), \tag{3}$$

$$Y(\delta_n, t_n) = \{1 + \epsilon_1[1 + \cos(t_n)]\}\sin(\delta_n). \tag{4}$$

where $\delta_n = \pi/2 + \theta_n + \arcsin[-b_n/R(t)]$ is the position of the particle on the boundary at nth collision as can be seen in Fig. 2(a). Starting at the position $[X(\delta_n, t_n), Y(\delta_n, t_n)]$, it is easy to see that the angle the particle's trajectory forms with the horizontal is $(\theta_n + \pi/2)$ [see Fig. 2(a)]. So, the vector velocity of the particle is written as

$$\vec{V}_n = |\vec{V}_n|[\cos(\theta_n + \pi/2)\hat{i} + \sin(\theta_n + \pi/2)\hat{j}], \tag{5}$$

where $\hat{i}$ and $\hat{j}$ represent the unit vectors with respect to the X and Y axis, respectively. The above expressions allow us to obtain the position of the particle as a function of time for $t \geq t_n$

$$X_p(t) = X(\delta_n, t_n) + |\vec{V}_n|\cos(\theta_n + \pi/2)(t - t_n), \tag{6}$$

$$Y_p(t) = Y(\delta_n, t_n) + |\vec{V}_n|\sin(\theta_n + \pi/2)(t - t_n). \tag{7}$$

The index p denotes that such coordinates correspond to the particle. In order to know the position of the particle at $(n+1)$th collision, we need to solve numerically $\sqrt{[l_x - X_p(t)]^2 + [l_y - Y_p(t)]^2} = R(t)$. This condition essentially means that the position of the particle is the same as the scatter and gives the instant of the collision. Additionally, l_x and l_y are the X and Y components of $l(s_n)$ and this distance is measured from the origin of the coordinates system to the center of the $s_n = 0, ..., 7$ scatter at $(n+1)$th collision and it takes different values according to s_n. Since the position of the particle at the collision $(n+1)$th is already known, one can easily obtain the distance between two successive impacts which is $d = \sqrt{[X_p(t) - X(\delta_n, t_n)]^2 + [Y_p(t) - Y(\delta_n, t_n)]^2}$. Once the velocity is constant between collisions, the time at the collision $(n+1)$th is obtained evaluating the expression

$$t_{n+1} = t_n + \frac{\sqrt{\Delta X^2 + \Delta Y^2}}{|\vec{V}_n|}. \tag{8}$$

where $\Delta X = X_p(t) - X(\delta_n, t_n)$ and $\Delta Y = Y_p(t) - Y(\delta_n, t_n)$. The impact parameter, b_{n+1}, which is perpendicular to the particle's trajectory, is obtained geometrically as can be seen in Fig. 2(b) and it is written as

$$b_{n+1} = b_n - l(s_n)\sin\left(\theta_n - \frac{\pi s_n}{4}\right). \tag{9}$$

Moreover, since t_{n+1} and b_{n+1} are already known, the new direction of the trajectory, θ_{n+1} [see Fig. 2(c)], is given by

$$\theta_{n+1} = \pi + \theta_n + 2\arcsin\left[\frac{b_{n+1}}{R(t_{n+1})}\right]. \tag{10}$$

We already know $(\theta_{n+1}, b_{n+1}, t_{n+1})$, however we still have to find $|\vec{V}_{n+1}|$. Since the reference frame of the boundary is moving, at the instant of the collision, and according to our construction, the following conditions must be satisfied:

$$\vec{V}'_{n+1} \cdot \vec{T}_{n+1} = \gamma \vec{V}'_n \cdot \vec{T}_{n+1}, \tag{11}$$

$$\vec{V}'_{n+1} \cdot \vec{N}_{n+1} = -\delta \vec{V}'_n \cdot \vec{N}_{n+1}, \tag{12}$$

where $\gamma \in [0, 1]$ and $\delta \in [0, 1]$ are damping coefficients. They mean that the particle has a fractional loss of energy upon each collision. The complete inelastic case occurs when $\gamma = \delta = 0$. On the other hand, when $\gamma = \delta = 1$ corresponds to the conservative case. The upper prime indicates that the velocity of the particle is measured with respect to the reference frame of the moving boundary.

Hence, after some easy algebra, one can find that

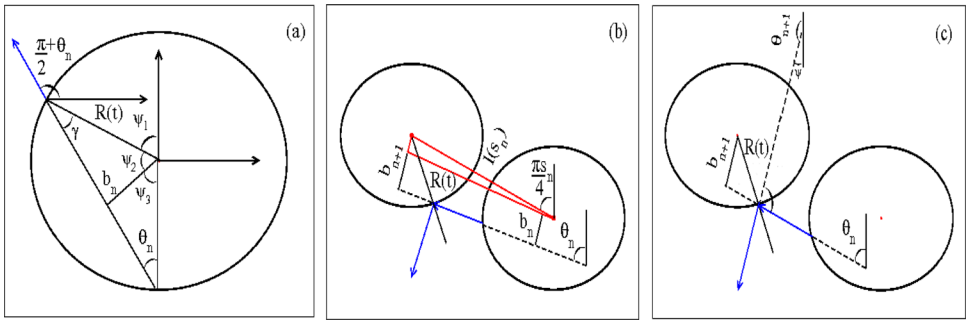

FIG. 2. (a) Position of the particle on the boundary for each collision; (b) b_{n+1} on b_n and θ_n; dependence of (c) θ_{n+1} on b_{n+1} and θ_n.

$$\vec{V}_{n+1}\cdot\vec{T}_{n+1}=\gamma|\vec{V}_n|\sin(\nu)-(1-\gamma)\epsilon_1\sin(t_{n+1}), \quad (13)$$

$$\vec{V}_{n+1}\cdot\vec{N}_{n+1}=-\delta|\vec{V}_n|\cos(\nu)+(1+\delta)\epsilon_1\sin(t_{n+1}), \quad (14)$$

where $\nu=\arcsin[-\mathrm{b_{n+1}}/\mathrm{R(t_{n+1})}]$. Finally, the velocity of the particle at $(n+1)$th collision is given by

$$|\vec{V}_{n+1}|=\sqrt{[\vec{V}_{n+1}\cdot\vec{T}_{n+1}]^2+[\vec{V}_{n+1}\cdot\vec{N}_{n+1}]^2}. \quad (15)$$

Now, we are able to describe the behaviour of a time dependent Lorentz gas with breathing time dependent perturbation.

A. Numerical results

In this section, we present our numerical results for a time-dependent Lorentz gas. We discuss basically the behaviour of the average velocity of the particle as a function of the number of collisions with the time dependent scatters. Considering the conservative dynamics $(\gamma=\delta=1)$, we study the influence of the initial velocity on the behaviour of the average velocity. On the other hand, for the dissipative dynamics, we consider different values of the dissipation parameter along the normal component of the velocity of the particle $\delta\neq 1$. Therefore, we apply two different procedures to obtain the average velocity. First, we evaluate the average velocity over the orbit for a single initial condition which is defined as

$$V_i=\frac{1}{n+1}\sum_{j=0}^{n}V_{i,j}, \quad (16)$$

where the index i corresponds to a sample of an ensemble of initial conditions and the average velocity over an ensemble of initial conditions is written as

$$\bar{V}=\frac{1}{M}\sum_{i=1}^{M}V_i, \quad (17)$$

where $M=1000$ denotes the number of different initial conditions.

1. Scaling invariance for different initial velocities

As part of our numerical results, in this section, we discuss the influence of the initial velocity on the behaviour of the average velocity, thus our main goal is to describe a scaling invariance observed for the conservative dynamics.[50] Therefore, we assume $\gamma=\delta=1$ in Eqs. (11) and (12). Figure 3 shows the behavior of the average velocity as a function of the number of collisions for ten different initial velocities. The control parameters used in Fig. 3 were $r_a=0.45, r_b=0.23, \epsilon_1=1.2\times10^{-2}$, and $\epsilon_2=10^{-3}$. For each curve, we fixed V_0 and the other variables were chosen randomly in the interval $t\in[0,2\pi], \theta\in[0,2\pi]$, and $b\in[-r_a,r_a]$. As one sees, all curves of the average velocity behave quite similarly. For short n, the average velocity remains constant, however, after a characteristic number n_x denoted as crossover number, all the curves start to grow

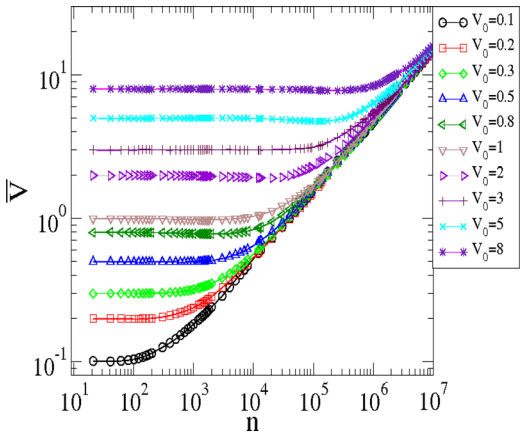

FIG. 3. Behaviour of $\bar{V}\times n$ for ten different initial velocities. The control parameters used were $r_a=0.45, r_b=0.23, \epsilon_1=1.2\times10^{-2}$, and $\epsilon_2=10^{-3}$.

together with the same slope.[51] Based on such behaviour, we propose the following:

(1) When $n\ll n_x$, the average velocity behaves according to

$$\bar{V}_{ip}\propto V_0^{\alpha}, \quad (18)$$

where ip means initial plateau and α is the exponent of the initial plateau. By construction, it must be $\alpha=1$;

(2) For $n\gg n_x$, the average velocity is given by

$$\bar{V}\propto n^{\beta}, \quad (19)$$

where β is the acceleration exponent; and

(3) The crossover number that marks the change from constant velocity to the growth regime is written as

$$n_x\propto V_0^{z}, \quad (20)$$

where z is the crossover exponent.

After considering the above initial assumptions, we suppose that the behaviour of the average velocity can be described in terms of a scaling function of the type

$$\bar{V}(V_0,n)=\tau\bar{V}(\tau^pV_0,\tau^qn), \quad (21)$$

where p and q are scaling exponents that in principle must be related to α, β, and z, and τ is the scaling factor. Given that τ is a scaling factor, we can chose $\tau^pV_0=1$, then we have $\tau=V_0^{-1/p}$. Moreover, Eq. (21) can be rewritten as

$$\bar{V}(V_0,n)=V_0^{-1/p}\bar{V}_1(V_0^{-q/p}n), \quad (22)$$

where the function $\bar{V}_1$ is defined as $\bar{V}_1(V_0^{-q/p}n)=\bar{V}(1,V_0^{-q/p}n)$ and is assumed to be constant for $n\ll n_x$. Comparing Eqs. (18) and (22), it is easy to see that $\alpha=-1/p$. On the other hand, choosing now $\tau=n^{-1/q}$, Eq. (21) can be rewritten as

$$\bar{V}(V_0,n)=n^{-1/q}\bar{V}_2(n^{-p/q}V_0), \quad (23)$$

where the function $\bar{V}_2$ is defined as $\bar{V}_2(n^{-p/q}V_0)=\bar{V}(n^{-p/q}V_0,1)$. It is also assumed to be constant for

$n \gg n_x$. Comparing Eqs. (19) and (23), we find $\beta = -1/q$. Finally, the expression for z, namely, the crossover exponent, can be obtained by using the two different expressions of the scaling factor τ, thus one obtain

$$z = \frac{\alpha}{\beta}. \tag{24}$$

Observe that the scaling exponents are determined if the exponents α and β are numerically obtained. The acceleration exponent β is obtained from a power law fitting for the average velocity when $n \gg n_x$. Thus, an average of these values gives us $\beta = 0.503(3)$. Figure 4 shows the behaviour of (a) $\bar{V}_{ip}$ vs. V_0 and (b) n_x vs. V_0. After power law fittings, we obtain $\alpha = 0.9995(1) \cong 1$ and $z = 1.986(3) \cong 2$. The crossover exponent z can also be obtained analytically by using the previous values of the acceleration exponent β and the exponent of the initial plateau α and Eq. (24). So, we find that $z = 1.987(9)$ which is in excellent agreement with our numerical data.

Once all the exponents are known, a final confirmation of the scaling behavior is given by the overlap of all the curves of the average velocity onto a single plot, as shown in Fig. 5. Such overlap confirms that the behaviour of the average velocity is scaling invariant under specific transformations. Additionally, such a result allows us to make a connection with Ref. 52, where the arrangement of the scatters, and the time dependent perturbation is different from

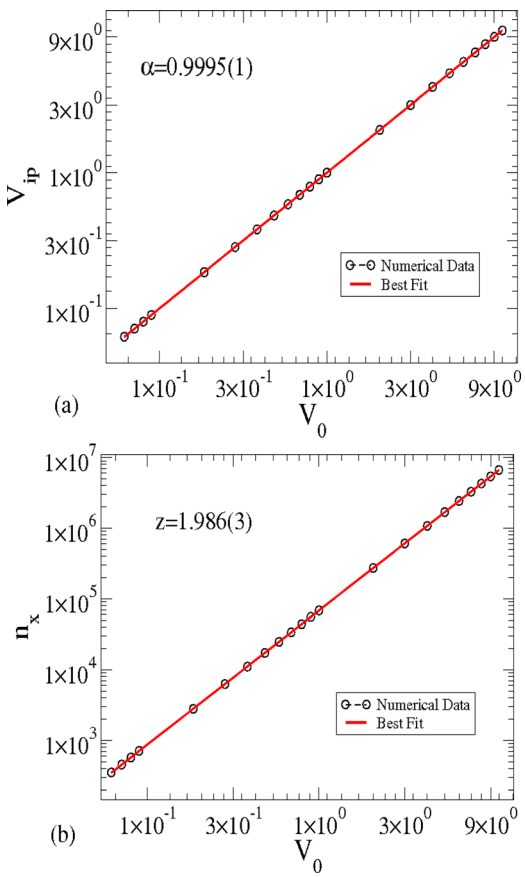

FIG. 4. (a) Behaviour of the velocity of the initial plateau V_{ip} as a function of V_0, where $\alpha = 0.9995(1)$. (b) Behaviour of the crossover as a function of the initial velocities. A power law fitting gives us $z = 1.986(3)$.

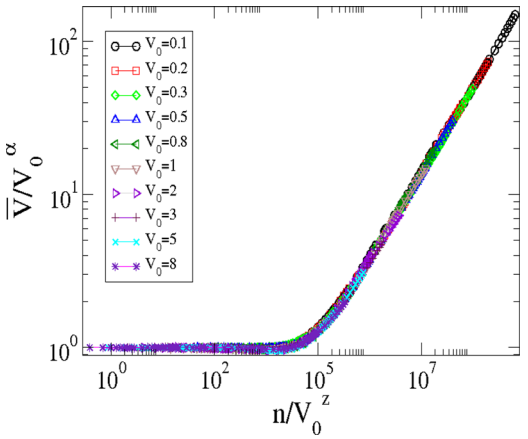

FIG. 5. Overlap of ten curves of the average velocity with different initial velocities onto a single and universal plot.

the present here. In Ref. 52, it is considered that the size of the scatters are all the same and does not change in time, but the position of the center of mass of each scatter does. It moves harmonically to the right and to the left, up and down, or as a combination of both (diagonal). However, the results presented in Ref. 52, and the results studied here for the conservative dynamics generates the same scaling exponents, namely, $\alpha \approx 1, \beta \approx 0.5$, and $z \approx 2$. Therefore, we conclude that the scaling invariance (and the scaling exponents) does not depend neither on the arrangement of the scatters nor the time dependent perturbation.

2. Scaling invariance for the case of collisional dissipation

In this section, we present our results for the dissipative dynamics of a time dependent Lorentz gas. Our main goal is to understand the influence of dissipation, namely, collisional dissipation, on the behaviour of the average velocity of the particle as a function of the number of collisions with the time dependent scatters. However, considering different values for the damping coefficient along the normal component of the particle's velocity, δ. Additionally, the dissipation parameter for the tangential component of the particle's velocity was fixed as $\gamma = 1$. Here, we use a scaling formalism in order to describe the transition from unlimited to limited energy growth. Indeed, such a transition happens when the dissipation parameter $\delta \to 1$, however it is better characterized by choosing the following transformation $\delta \to (1 - \delta)$.

To obtain the average velocity, we fixed the control parameters $r_a = 0.45$ and $r_b = 0.23$ and each initial condition has a fixed initial velocity, $V_0 = 10^{-3}$ and (θ_0, b_0, t_0) were randomly chosen in the interval $\theta \in [0, 2\pi], t \in [0, 2\pi]$, and $b \in [-r_a, r_a]$.

Figure 6 shows the behaviour of the average velocity as function of the number of collisions for different values of the damping coefficient δ. Observe that, for different values of δ and for small number of collisions, all the curves for the average velocity start to grow with the same exponent and they bend towards a regime of saturation for large enough values of n. We see also that the stronger the dissipation, the

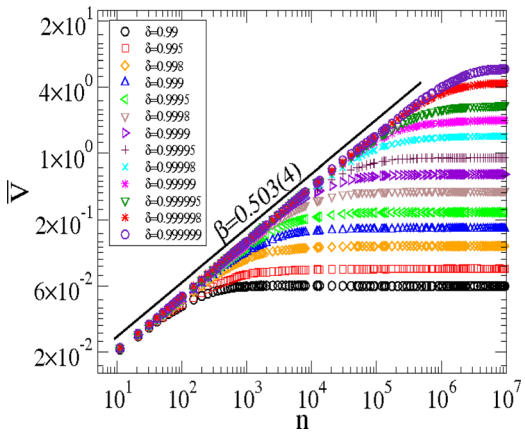

FIG. 6. Behaviour of $\bar{V}$ vs. n for different values of δ, as labeled in the figure.

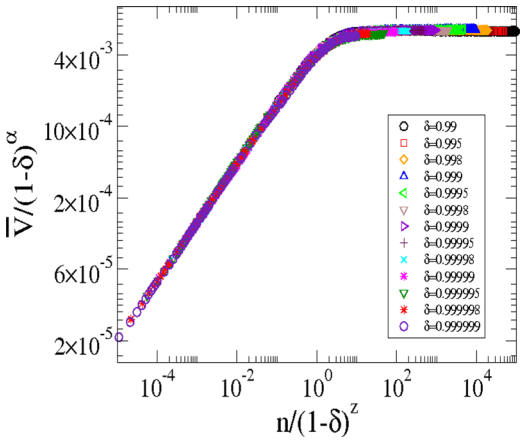

FIG. 7. Overlap of different curves of the average velocity as a function of the number of collisions for ten different values of the dissipation parameter δ onto a single plot. Here, we have considered the case of collisional dissipation.

faster is the saturation. The changeover from growth to the saturation is marked by a typical crossover number n_x obtained by the intersection of the acceleration line and the saturation line. We propose the following scaling hypotheses:

(1) When $n \ll n_x$, the average velocity is

$$\bar{V} \propto n^{\beta}, \tag{25}$$

where β is the acceleration exponent;

(2) For long time, $n \gg n_x$, the average velocity approaches a regime of saturation, which is described as

$$\bar{V}_{sat} \propto (1-\delta)^{\alpha}, \tag{26}$$

where α is the saturation exponent; and

(3) The crossover number that marks the transition from growth to the constant velocity is written as

$$n_x \propto (1-\delta)^{z}, \tag{27}$$

where z is the crossover exponent.

After an extensive numerical investigation along the range $\delta \in [0.99, 0.999999]$, we obtain that $\beta = 0.503(4)$. The saturation exponent α is obtained by a power law fitting for the value of the saturation velocity as $\alpha = -0.5033(2)$. Finally, the crossover exponent z is obtained by a power law fitting for the value of the crossover number as a function of $(1-\delta)$ as $z = -1.000(5)$. The crossover exponent can also be obtained analytically given that the acceleration exponents and the saturation exponent are known. Using similar procedure as made in Sec. II A 1, we have

$$z = \frac{\alpha}{\beta} = -1.000(8), \tag{28}$$

which is in good agreement with the value obtained numerically. Once all the exponents are known, a confirmation of the initial hypotheses is made overlapping all curves of $\bar{V}$ vs. n onto a single plot as shown in Fig. 7. Such a result allows us to confirm that the system is scaling invariant under a specific transformation and also that the introduction of collisional dissipation causes a drastic change in the behavior of $\bar{V}$. The unlimited energy growth present in the conservative dynamics is no longer observed. Observe that both α and z are negative, which lead to $V_{sat} \propto (1-\delta)^{-0.5033(2)}$ and $n_x \propto (1-\delta)^{-1.000(5)}$. Note that when $\delta \to 1$ implies that $\bar{V}_{sat} \to \infty$ and $n_x \to \infty$, too, thus recovering the results for the conservative case, i.e., Fermi acceleration. However, when δ is slightly smaller than 1, it implies that the system possesses a characteristic saturation value $\bar{V}_{sat}$ and a crossover iteration number n_x. Our results for a two dimensional time-dependent billiard confirm that collisional dissipation is a sufficient condition to suppress the unlimited energy growth. Additionally, given that the values of the exponents are: the acceleration exponent $\beta \approx 0.5$, the saturation exponent $\alpha \approx -0.5$, and the crossover exponent $n_x \approx -1$, we conclude that, in spite of all their differences, the time dependent Lorentz gas with collisional dissipation belongs to the same class of universality of the one dimensional bouncer model.[53] Additionally, such results reinforce the scaling exponents neither depend on the arrangement of the scatters nor the time dependent perturbation, since such exponents were the same observed in Ref. 52 for the dissipative dynamics.

III. IN-FLIGHT DISSIPATION

In this section, we consider a Lorentz gas with the same kind of time dependent perturbation as presented in Sec. II A 2, however instead of consider inelastic collisions, we introduce in-flight dissipation into the model. First, we assume that the particle is immersed and moving in a fluid. Thus, the dissipation considered is proportional to a power of the velocity of the particle V. We consider three different types of dissipation laws, namely: (1) $F = -\eta' V^2$ and (2) $F = -\eta' V^{\mu}$ with $\mu \neq 1$ and $\mu \neq 2$; and (3) $F = -\eta' V$, where η' is the dissipation parameter. Again, we have a two dimensional system described in terms of a four dimension nonlinear map. The expressions for both b_{n+1} and θ_{n+1} do not change, and they are given by Eqs. (9) and (10), respectively. However, (V_{n+1}, t_{n+1}) must be found. To obtain the equation

that describes the velocity of the particle along its trajectory, we have to solve Newton's equation. Here, we explain in details the procedure to obtain the map for case (i), however, the extension for cases (ii) and (iii) is straightforward. Thus, we have $F = -\eta' V^2 = mdV/dt$ with the initial velocity $|\vec{V}_n| > 0$, and η' is the coefficient of the drag force. After introducing the variables $\eta'/m = \eta$, we obtain the velocity of the particle as function of time as

$$|\vec{V}_p(t)| = \frac{V_n}{1 + V_n\eta(t - t_n)}, \tag{29}$$

where $V_n = |\vec{V}_n|$. The particle travels on a straight line until it hits one of the other 12 neighboring scatters. Integration of Eq. (29) gives that the displacement of the particle is given by

$$r(t) = \frac{\ln[1 + V_n\eta(t - t_n)]}{\eta}. \tag{30}$$

Observe that the dissipation does not stop the dynamics of the particle, since $r(t)$ grows as the time increases, $t > t_n$. The dynamics of the particle is followed by molecular dynamics until the particle hits the scatter. The time at that point is obtained evaluating $t_{n+1} = t_n + t_c$, where t_c is the time during the flight. To obtain the new velocity, we should note that the referential frame of the boundary is moving, then, at the instant of the collision, the following conditions must be satisfied:

$$\vec{V}'_{n+1} \cdot \vec{T}_{n+1} = \vec{V}'_p \cdot \vec{T}_{n+1}, \tag{31}$$

$$\vec{V}'_{n+1} \cdot \vec{N}_{n+1} = -\vec{V}'_p \cdot \vec{N}_{n+1}, \tag{32}$$

where the upper prime indicates that the velocity of the particle is measured with respect to the moving boundary referential frame, and the vectors $\vec{T}$ and $\vec{N}$ are the unitary tangent and normal vectors, respectively. Hence, one can easily find that

$$\vec{V}_{n+1} \cdot \vec{T}_{n+1} = |\vec{V}_p| \sin(\nu), \tag{33}$$

$$\vec{V}_{n+1} \cdot \vec{N}_{n+1} = -|\vec{V}_p| \cos(\nu) + 2\epsilon_1 \sin(t_{n+1}), \tag{34}$$

where $\nu = \arcsin[-b_{n+1}/R(t_{n+1})]$.

Finally, the velocity at $(n+1)$th collision is given by

$$|\vec{V}_{n+1}| = \sqrt{(\vec{V}_{n+1} \cdot \vec{T}_{n+1})^2 + (\vec{V}_{n+1} \cdot \vec{N}_{n+1})^2}. \tag{35}$$

With this four dimensional mapping, we can explore now numerical results for the dynamics of the particle experiencing dissipation during the flight.

A. Numerical results for the case of in-flight dissipation

In this section, we discuss our numerical results for the time-dependent Lorentz gas considering the effects of in-flight dissipation. The procedure applied is the same used in the previous sections, mainly we consider the behaviour of the average velocity for an ensemble of $M = 10^3$ initial condition (see Eqs. (16) and (17)) as a function of the number of collision considering different values of the parameter η. In our simulation, we have considered $\eta \in [10^{-4}, 10^{-2}]$ and fixed $V_0 = 10^{-3}$, randomly chosen $t \in [0, 2\pi]$, $\theta \in [0, 2\pi]$, and $b \in [-r_a, r_a]$, and $r_a = 0.45, r_b = 0.23, \epsilon_1 = 1.2 \times 10^{-2}$, and $\epsilon_2 = 10^{-3}$.

1. Numerical results for the case $F = -\eta V^2$

Figure 8 shows the behaviour of the average velocity as a function of the number of collisions for different values of η. Observe that, for short n, all the average velocity for different values of η starts to grow together and then it bends towards a regime of saturation for long enough values of n. Additionally, the stronger is the dissipation, the faster is the saturation regime. The behavior observed in Fig. 8 can be described by

(1) When $n \ll n_x$, the average velocity is

$$\bar{V}(n, \eta) \propto n^{\beta}, \tag{36}$$

where the exponent β is called the acceleration exponent.

(2) When $n \gg n_x$, the average velocity is described as

$$\bar{V}_{sat} \propto \eta^{\alpha}, \tag{37}$$

where α is the saturation exponent.

(3) The change from growth to the saturation $(n \approx n_x)$ is supposed to scale as

$$n_x \propto \eta^{z}, \tag{38}$$

where z is called the crossover exponent.

A power law fitting in Fig. 8 for $n \ll n_x$ gives us that $\beta = 0.501(4)$. Such value was obtained from the range of $\eta \in [10^{-4}, 10^{-2}]$. The saturation exponent $\alpha = 0.501(2)$ is obtained by a power law fitting of V_{sat} vs. η, and the crossover exponent $z = -1.000(3)$ is obtained by a power law fitting of

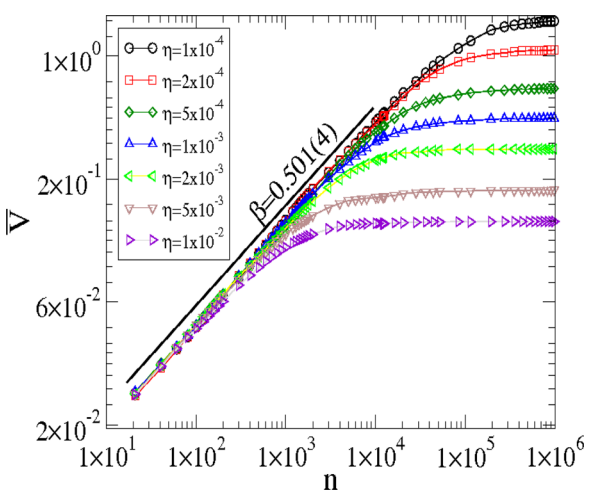

FIG. 8. Behaviour of $\bar{V}$ vs. n for the case $F = -\eta V^2$ for different values of η, as labeled in the figure.

n_x vs. η and, therefore, is very close to $z = \alpha/\beta = -1.00(1)$. Finally, a confirmation of the initial hypotheses is made by the overlap of all the curves of $\bar{V}$ vs. n onto a single plot as shown in Fig. 9. With this overlap of all the curves of the average velocity and considering that values for the exponents are $\beta \cong 0.5$, $\alpha \cong -0.5$, and $z \cong -1$, we can conclude that the dissipative one dimensional bouncer model,[53] the time dependent Lorentz gas with collisional and of in-flight dissipation due to a drag force ($F = -\eta V^2$) and the dissipative time dependent oval billiard also under the effects of dissipation due to a drag force[54] belong to the same class of universality. Additionally, the introduction of in-flight dissipation due to a drag force is also a sufficient condition to suppress the unlimited energy growth.

2. Numerical results for the case $F = -\eta V^{\mu}$ with $1<\mu<2$

In this section, we consider the case (ii), i.e., $F = -\eta V^{\mu}$ with $1 < \mu < 2$. Solving Newton's law $F = -\eta V^{\mu} = dV/dt$ with the $V_n > 0$, we obtain the velocity of the particle as function of time as

$$V_p(t) = [V_n^{1-\mu} - \eta(1-\mu)(t-t_n)]^{\frac{1}{1-\mu}}, \tag{39}$$

where $V_n = \mid \vec{V}_n \mid, t > t_n$ and $\mu \neq 1$. The displacement of the particle is obtained by the integration of $dr/dt = V_p(t)$, which gives

$$r(t) = \frac{V_n^{2-\mu}}{\eta(2-\mu)} - \frac{[V_n^{1-\mu} - \eta(1-\mu)(t-t_n)]^{\frac{2-\mu}{1-\mu}}}{\eta(2-\mu)}, \tag{40}$$

with $t > t_n, \mu \neq 1$, and $\mu \neq 2$. The limit of $\mu \to 1$ and $\mu \to 2$ in Eqs. (39) and (40) can be obtained easily. First, let us consider the case of $\mu \to 2$, thus, expanding Eqs. (39) and (40) in series and taking only terms of first order, we obtain

$$V_p(t) = \frac{V_n}{1 + V_n\eta(t-t_n)} + \bigcirc(\mu - 2) \tag{41}$$

$$r(t) = \frac{\ln[1 + V_n\eta(t-t_n)]}{\eta} + \bigcirc(\mu - 2), \tag{42}$$

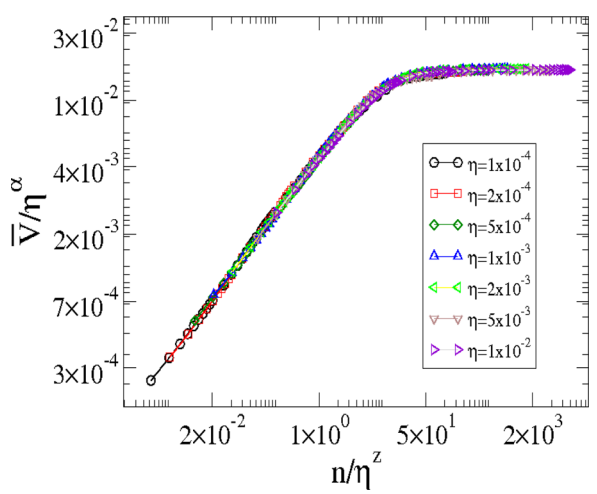

FIG. 9. Overlap of different curves of the $\bar{V}$ for seven different values of the dissipation parameter η onto a single plot for the case $F = -\eta V^2$.

which corresponds to the case $F = -\eta V^2$, considered in Sec. III A 1. On the other hand, considering now the limit case of $\mu \to 1$ and proceeding in the same way, we obtain

$$V_p(t) = V_n e^{-\eta(t-t_n)} + \bigcirc(\mu - 1), \tag{43}$$

$$r(t) = V_n \frac{[1 - e^{-\eta(t-t_n)}]}{\eta} + \bigcirc(\mu - 1). \tag{44}$$

The above expressions, as we will see, correspond to the case $F = -\eta V$ and will be treated in Sec. III A 3. Here, it is important to emphasize that depending on the control parameter μ, the dissipation stops completely the dynamics of the particle. In order to illustrate such a behaviour, we show in Fig. 10 the fraction of initial conditions that come to stop (f) as a function of the control parameter μ. The function f is obtained by using an ensemble of 1000 initial conditions (see Eqs. (16) and (17)) iterated up to $n = 10^6$. We fixed $V_0 = 10$ and $\eta = 10^{-2}$, and the other variables were chosen randomly in the interval $t \in [0, 2\pi], \theta \in [0, 2\pi]$, and $b \in [-r_a, r_a]$. Observe that for values of $\mu < 1.26$, all the particles stop and on the other hand, for values of $\mu > 1.49$, none of the initial conditions reach the rest due to the dissipation, at least for $n = 10^6$ and for values of $1.26 < \mu < 1.49$, the function f decays monotonically, as shown in Fig. 10. Therefore, let us extend our results presented in the Sec. III A 1 for the case $F = -\eta V^2$. Here, we study the behaviour of the average velocity as a function of the number of collisions with the time dependent scatters considering different values for the coefficient of the dissipative force η as well as different values of μ. We performed our simulations for values of $\mu \in [1.5, 1.99]$ and observed a similar behaviour as shown in Fig. 8, and such a behaviour can be describe by using the scaling hypotheses given by Eqs. (36)–(38). The acceleration exponent is $\beta \approx 0.5$ for all the values of μ. However, the saturation exponent α and the crossover exponent z are rather different. Table I shows the value for the exponents β, α and the numerical value of z as well as the values obtained by using the expression $z = \alpha/\beta$,

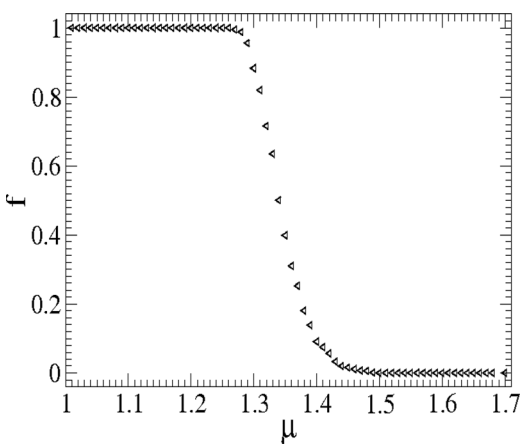

FIG. 10. Fraction of initial conditions that came to stop (f) as a function of μ. Here, we have considered in our simulations $\eta = 10^{-2}$ and $n = 10^6$ collisions. Observe that for values of $\mu < 1.26$, all the particles stop, and on the other hand, for values of $\mu > 1.49$, none of the initial conditions reach the rest due to the dissipation, at least for $n = 10^6$.

TABLE I. Exponents α, β, and z obtained for different values of μ as labeled in the table.

μ	β	α	$z_{numerical}$	$z = \alpha/\beta$
1.50	0.499(3)	−0.679(2)	−1.367(9)	−1.36(1)
1.55	0.500(3)	−0.652(1)	−1.299(8)	−1.304(9)
1.60	0.500(1)	−0.629(1)	−1.255(5)	−1.258(4)
1.65	0.500(2)	−0.622(5)	−1.239(3)	−1.24(1)
1.70	0.500(2)	−0.596(1)	−1.192(7)	−1.192(6)
1.75	0.502(1)	−0.568(8)	−1.131(3)	−1.13(1)
1.80	0.500(2)	−0.560(2)	−1.128(4)	−1.120(8)
1.85	0.501(3)	−0.550(2)	−1.088(8)	−1.09(1)
1.90	0.501(2)	−0.526(2)	−1.047(9)	−1.049(6)
1.95	0.499(2)	−0.516(2)	−1.028(8)	−1.034(8)
1.99	0.501(1)	−0.505(2)	−1.003(7)	−1.007(6)
2.00	0.501(4)	−0.501(2)	−1.000(3)	−1.00(1)

and as can be seen, they are in perfect agreement. Note also that, as $\mu \to 2$, the exponent $\alpha \to -0.5$ and $z \to -1$. Finally, in order to confirm our scaling hypotheses and the validity of our exponents, we show in Fig. 11 an overlap of seven curves for the average velocity considering different values of the dissipation parameter η and for four different values of parameter μ.

3. Numerical results for the case $F = -\eta V$

Finally, we consider case (iii), where $F = -\eta V$. For such a case, the velocity of the particle as a function of time is given by

$$V_p(t) = V_n e^{-\eta(t-t_n)}, \tag{45}$$

and the distance that the particle travels is

$$r(t) = V_n \frac{[1 - e^{-\eta(t-t_n)}]}{\eta}, \tag{46}$$

We have shown in Fig. 10 that the dynamics of the particle will eventually stop for values of $\mu < 1.26$ (see Eqs. (39) and (40)), therefore it is also expected to happen here. Therefore, we have studied the behaviour of the decay of the average velocity for an ensemble of $M = 10^3$ different initial conditions for this case (see Eqs. (16) and (17)) as we did for the previous ones. Figure 12(a) shows the behaviour of $\bar{V}$ vs. n for different values of η and for a fixed initial velocity $V_0 = 10$. Observe that for small number of collisions, the decay is linear, and then there is a crossover and a faster linear decay until the dynamics completely stop after the second crossover. It is important to mention that this second decay is observed only for strong dissipation $(\eta > 10^{-3})$, for values of $(\eta < 10^{-3})$, we can not differ the second from the first decay. Additionally, the stronger is the dissipation, the faster the particle comes to stop. Figure 12(b) shows the slope of the decay for the average velocity for the first region as a function of η. Applying a linear fit, we obtained $Y \approx -0.05720(5)\eta$, where 5×10^{-5} represents the error of the fitting. Such a result allows us to compare our systems with two other models, namely, the one dimensional Fermi-Ulam model and the two-dimensional time-dependent oval billiard. The Fermi-Ulam model[55] consists of a classical

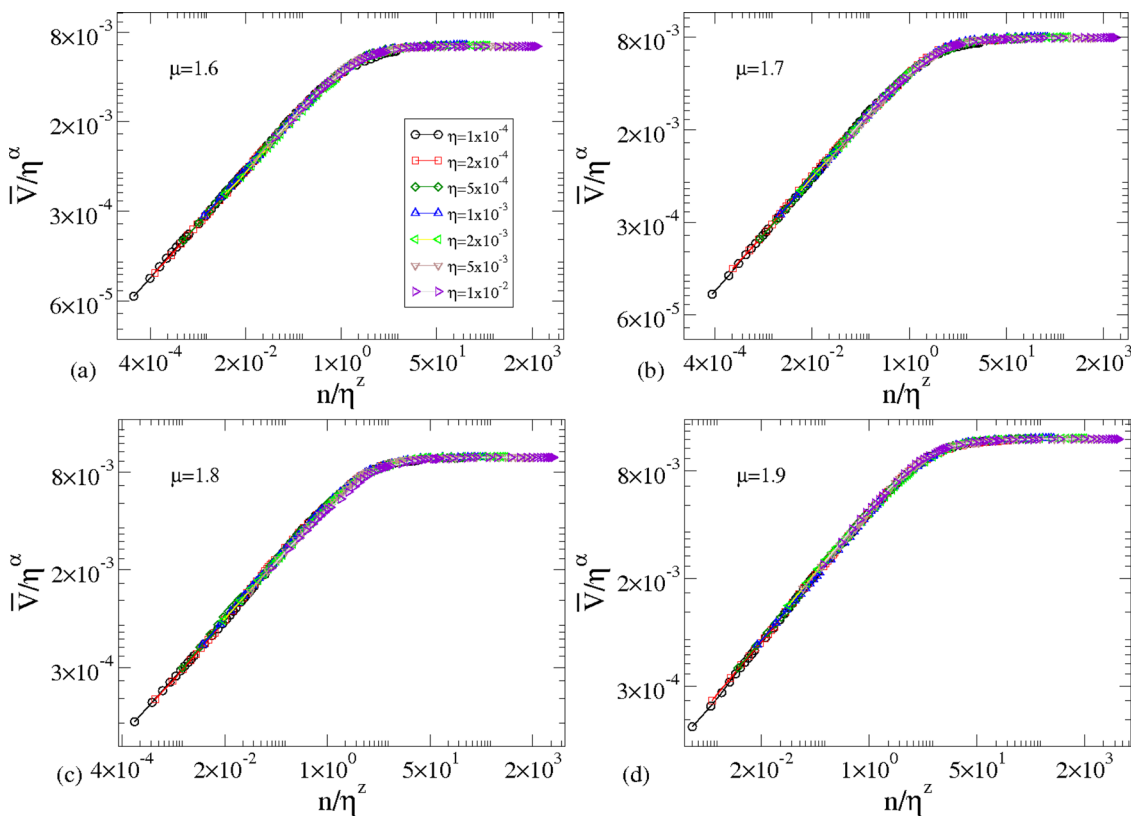

FIG. 11. Overlap of all the curves for the average velocity for different values for μ. The control parameters used were: (a) $\mu = 1.6$, (b) $\mu = 1.7$, (c) $\mu = 1.8$, and (d) $\mu = 1.9$. The values for the saturation exponents α and the crossover exponents z are shown in Table I.

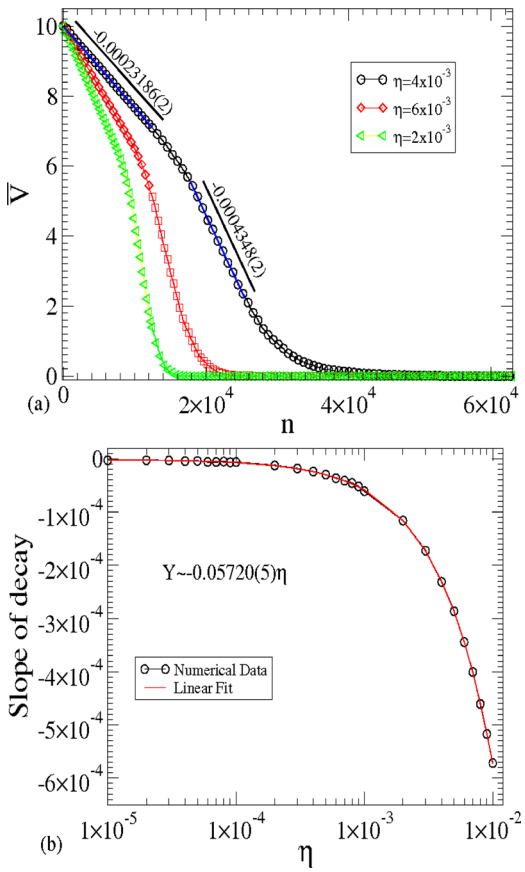

FIG. 12. (a) Behaviour of the average velocity as a function of the number of collisions n for different values of η. (b) The slope of decay of $\bar{V}$ vs. η, a linear fit gives us $Y \approx -0.05720(5)\eta$.

particle of mass m confined between two rigid walls, one of them is assumed to be fixed, while the other one moves periodically in time. For such a model, it was shown analytically that the decay of the particle's velocity is linearly dependent on the dissipation parameter η, i.e., $V_n \propto V_0 - 2n\eta$ (see Ref. 55). On the other hand, it was recently shown for the time dependent oval billiard,[54] which cloud be considered as a generalization of the Fermi-Ulam model, that the average particle's velocity decays slower. However, the behaviour is still linearly dependent on the dissipation parameter η, i.e., $V_n \propto V_0 - 1.5314(3)n\eta$ (see Ref. 54). Finally, the decay of the average velocity for the time depend Lorentz gas is also linearly dependent on η, i.e., $V_n \propto V_0 - 0.05720(5)n\eta$. Therefore, the dynamics of the particle will come to rest, however, much slower than the two other two systems.

IV. CONCLUSIONS

We studied the problem of non-interacting particles in a time dependent Lorentz gas considering the conservative as well as the dissipative dynamics. Our results for the conservative dynamics confirm the unlimited energy growth of the particle. Additionally, we have shown that the behaviour of the average velocity can be described by using scaling arguments. For the dissipative dynamics, we considered four different kinds of damping forces namely, one case of collisional dissipation and three cases of in-flight dissipation, namely, (i) $F = -\eta V^2$, (ii) $F = -\eta V^\mu$ with $\mu \neq 1$ and $\mu \neq 2$, and (iii) $F = -\eta V$, where η is the dissipation parameter. We have shown that the introduction of collisional dissipation is a sufficient condition to suppress the Fermi acceleration and that the behaviour of the average velocity for different values of the dissipation parameter along the normal component of the velocity is scaling invariant. Our results are compared those obtained for other different time perturbation in the Lorentz gas[52] for two different arrangement of the scatterers (triangular and square configuration) considering both the conservative as well as the case of collisional dissipation. Despite of their differences, the scaling exponents are the same, namely: the acceleration exponent is $\simeq 0.5$, the exponent of the initial plateau $\simeq 1$, and the crossover exponent is $\simeq 2$ for the conservative dynamics. On the other hand, for the case of collisional dissipation, the scaling exponents are: the acceleration exponent $\simeq 0.5$, the saturation exponent $\simeq 0.5$, and the crossover exponent $\simeq -1$. Thus, the scaling invariance and the scaling exponents neither depend on how the scatterers are organized nor the time dependent perturbation. Finally, we considered the case of in-flight dissipation, for all the cases, we studied the behaviour of the average velocity of one ensemble of initial conditions. Our results shown that, for some cases ($\mu \geq 1.5$) and for short number of collisions, the average velocity grows according to a power law, and after a characteristic crossover number, it remains constant. Therefore, confirming that the introduction of dissipation is a sufficient condition to suppress the unlimited energy growth also for the case of dissipation during the flight. On the other hand, for same cases ($\mu < 1.5$), the dissipation is so strong that, even for high initial velocities, the average velocity decay linearly until the particle come to stop between the scatterers.

ACKNOWLEDGMENTS

D.F.M.O. gratefully acknowledges the financial support by the Slovenian Human Resources Development and Scholarship Fund (Ad futura Foundation) and Max-Planck-Institut für Physik komplexer Systeme for the kind hospitality during his visit. E.D.L. acknowledges the financial support by FAPESP, CNPq, and FUNDUNESP, Brazilian agencies. This research was supported by resources supplied by the Center for Scientific Computing (NCC/GridUNESP) of the São Paulo State University (UNESP).

[1]E. Fermi, Phys. Rev. **75**, 1169 (1949).
[2]S. E. Sklarz, D. J. Tannor, and N. Khaneja, Phys. Rev. A **69**, 053408 (2004).
[3]R. Gommers, S. Bergamini, and F. Renzoni, Phys. Rev. Lett. **95**, 073003 (2005).
[4]M. Steiner, M. Freitag, V. Perebeinos, J. C. Tsang, J. P. Small, M. Kinoshita, D. Yuan, J. Liu, and P. Avouris, Nat. Nanotechnol. **4**, 320 (2009).
[5]K. Nakamura and T. Harayama, *Quantum Chaos and Quantum Dots* (Oxford University Press, Oxford, 2004).
[6]D. G. Ladeira and J. K. L. da Silva, Phys. Rev. E **73**, 026201 (2006).
[7]E. D. Leonel, J. K. L. da Silva, and S. O. Kamphorst, Physica A **331**, 435 (2004).
[8]A. K. Karlis, P. K. Papachristou, F. K. Diakonos, V. Constantoudis, and P. Schmelcher, Phys. Rev. Lett. **97**, 194102 (2006).
[9]A. K. Karlis, P. K. Papachristou, F. K. Diakonos, V. Constantoudis, and P. Schmelcher, Phys. Rev. E **76**, 016214 (2007).
[10]J. V. José and R. Cordery, Phys. Rev. Lett. **56**, 290 (1986).

[11]A. D. Pustylnikov, Mat. Sb. **185**, 113 (1994); Russ. Acad. Sci. Sb. Math. **82**, 231 (1995).
[12]S. Ulam, in *Proceedings of the Fourth Berkeley Symposium on Math., Statistics and Probability* (University of California Press, Berkeley, 1961), Vol. 3, p. 315.
[13]A. J. Lichtenberg and M. A. Lieberman, Phys. Rev. A **5**, 1852 (1972).
[14]R. Douady, "Application du Theoreme des Tores Invariants," These de 3eme Cycle, University of Paris VII, 1982.
[15]A. D. Pustylnikov, Theor. Math. Phys. **50**, 449 (1995).
[16]A. D. Pustylnikov, Theor. Math. Phys. **57**, 1035 (1983).
[17]P. J. Holmes, J. Sound Vib. **84**, 173 (1982).
[18]R. M. Everson, Physica D **19**, 355 (1986).
[19]G. A. Luna-Acosta, Phys. Rev. A **42**, 7155 (1990).
[20]T. L. Vincent and A. I. Mees, J. Bifurcation Chaos **10**, 579 (2000).
[21]A. C. J. Luo, ASME J. Vib. Acoust. **124**, 420 (2002).
[22]A. C. J. Luo and R. P. S. Han, Nonlinear Dyn. **10**, 1 (1996).
[23]C. P. Dettmann and O. Georgiou, Physica D **238**, 2395 (2009).
[24]C. P. Dettmann and O. Georgiou, J. Phys. A.: Math. Theor. **44**, 195102 (2011).
[25]M. V. Berry, Eur. J. Phys. **2**, 91 (1981).
[26]N. Saitô, H. Hirooka, J. Ford, F. Vivaldi, and G. H. Walker, Physica D **5**, 273 (1982).
[27]E. G. Altmann, Phys. Rev. A **79**, 013830 (2009).
[28]S. O. Kamphorst and S. Pinto de Carvalho, Nonlinearity **12**, 1363 (1999).
[29]J. Koiller, R. Markarian, S. O. Kamphorst, and S. Pinto de Carvalho, J. Stat. Phys. **83**, 127 (1996).
[30]L. A. Bunimovich, Commun. Math. Phys. **65**, 295 (1979).
[31]Y. G. Sinai, Russ. Math. Surveys **25**, 137 (1970).
[32]N. Saitô, H. Hirooka, J. Ford, F. Vivaldi, and G. H. Walker, Physica D **5**, 273 (1982).
[33]M. Robnik, J. Phys. A **16**, 3971 (1983).
[34]M. V. Berry and M. Robnik, J. Phys. A **17**, 2413 (1984).
[35]M. Robnik and M. V. Berry, J. Phys. A **18**, 1361 (1985).
[36]R. Markarian, S. O. Kamphorst, and S. P. de Carvalho, Commun. Math. Phys. **174**, 661 (1996).
[37]V. Lopac, I. Mrkonjić, and D. Radić, Phys. Rev. E **59**, 303 (1999).
[38]V. Lopac, I. Mrkonjić, and D. Radić, Phys. Rev. E **66**, 036202 (2001).
[39]E. D. Leonel and P. V. E. McClintock, J. Phys. A **38**, 823 (2005).
[40]A. M. Ozorio de Almeida, *Hamiltonian Systems: Chaos and Quantization* (Cambridge University Press, Cambridge, 1988).
[41]Such an idea of unlimited energy growth comes from 1949 when Enrico Fermi, tried to explain the origin of cosmic ray acceleration proposed that charged particles could be accelerated by interaction with a time-dependent magnetic structures in the space.[1]
[42]A. Loskutov, A. R. Ryabov, and L. G. Akinshin, J. Phys. A **33**, 7973 (2000).
[43]F. Lenz, F. K. Diakonos, and P. Schmelcher, Phys. Rev. Lett. **100**, 014103 (2008).
[44]E. D. Leonel and L. A. Bunimovich, Phys. Rev. Lett. **104**, 224101 (2010).
[45]D. F. M. Oliveira and M. Robnik, Phys. Rev. E **83**, 026202 (2011).
[46]E. D. Leonel, J. Phys. A **40**, F1077 (2007).
[47]P. L. Garrido and G. Gallavotti, J. Stat. Phys. **76**, 549 (1994).
[48]P. L. Garrido, J. Stat. Phys. **88**, 807 (1997).
[49]D. P. Sanders, Phys. Rev. E **71**, 016220 (2005).
[50]E. D. Leonel, P. V. E. McClintock, and J. K. L. da Silva, **93**, 014101 (2004).
[51]Such a behaviour can be explained by suggesting that velocity does random walk with reflection from zero.
[52]D. F. M. Oliveira, J. Vollmer, and E. D. Leonel, Physica D **240**, 389 (2011).
[53]E. D. Leonel and A. L. P. Livorati, Physica A **387**, 1155 (2008).
[54]E. D. Leonel and L. A. Bunimovich, Phys. Rev. E **82**, 016202 (2010).
[55]E. D. Leonel and P. V. E. McClintock, J. Phys. A **39**, 11399 (2006).